Gold on Different Manganese Oxides: Ultra-Low-Temperature CO Oxidation over Colloidal Gold Supported on Bulk-MnO₂ Nanomaterials

Dong Gu,[†] Jo-Chi Tseng,[†] Claudia Weidenthaler,[†] Hans-Josef Bongard,[†] Bernd Spliethoff,[†] Wolfgang Schmidt,[†] Fouad Soulimani,[‡] Bert M. Weckhuysen,[‡] and Ferdi Schüth*,[†]

[†]Max-Planck-Institut für Kohlenforschung, Kaiser-Wilhelm-Platz 1, 45470 Mülheim an der Ruhr, Germany

[‡]Inorganic Chemistry and Catalysis, Debye Institute for Nanomaterials Science, Utrecht University, Universiteitsweg 99, 3584 CG Utrecht, The Netherlands

Ⓢ *Supporting Information*

ABSTRACT: Nanoscopic gold particles have gained very high interest because of their promising catalytic activity for various chemicals reactions. Among these reactions, low-temperature CO oxidation is the most extensively studied one due to its practical relevance in environmental applications and the fundamental problems associated with its very high activity at low temperatures. Gold nanoparticles supported on manganese oxide belong to the most active gold catalysts for CO oxidation. Among a variety of manganese oxides, Mn_2O_3 is considered to be the most favorable support for gold nanoparticles with respect to catalytic activity. Gold on

MnO_2 has been shown to be significantly less active than gold on Mn_2O_3 in previous work. In contrast to these previous studies, in a comprehensive study of gold nanoparticles on different manganese oxides, we developed a gold catalyst on MnO_2 nanostructures with extremely high activity. Nanosized gold particles (2−3 nm) were supported on $α$-MnO_2 nanowires and mesoporous $β$-MnO_2 nanowire arrays. The materials were extremely active at very low temperature (−80 °C) and also highly stable at 25 °C (70 h) under normal conditions for CO oxidation. The specific reaction rate of 2.8 $mol_{CO} \cdot h^{-1} \cdot g_{Au}^{-1}$ at a temperature as low as −85 °C is almost 30 times higher than that of the most active Au/Mn_2O_3 catalyst.
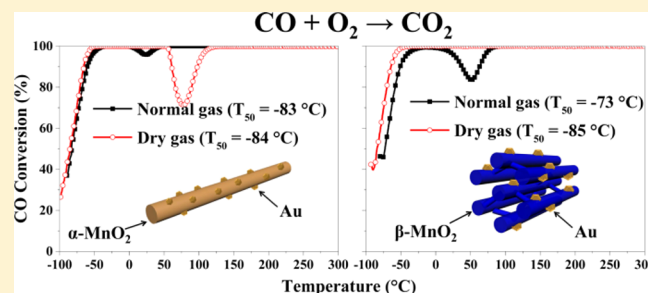
1. INTRODUCTION

Supported gold nanoparticles (GNPs) have triggered enormous research activities in the past decades because of their fascinating properties and related reactivity in various catalytic reactions.[1−6] Among these the low-temperature CO oxidation is of great interest due to its relevance in practical applications (such as in CO removal from hydrogen feed of polymer-electrolyte-membrane fuel cells (PEMFC), exhaust gas, and environmental air cleaning and sensing) and as a model reaction for the understanding of catalytic mechanisms.[7−9] Gold nanoparticles with particle sizes below 5 nm and highly dispersed on metal oxides (such as TiO_2,[1,3,6,10] Fe_2O_3,[11,12] CeO_2,[13,14] Co_3O_4,[15] Mn_2O_3,[16] $Mg(OH)_2$,[17,18] and MgO[17]) are known to be very active catalysts for CO oxidation at low temperatures. However, there are only few examples which show appreciable rates at temperatures below −70 °C. Gold clusters with sizes below 1 nm supported on $Mg(OH)_2$ were reported to be active at such low temperatures.[18] However, this low temperature activity was completely lost after calcination as the gold particle sizes increased to 3−5 nm during this calcination process. Therefore, the authors suggested that the high activity would be caused by gold clusters with sizes smaller than 1 nm. More recently, our group found that colloidally

deposited GNPs with particle sizes between 2−5 nm supported on $Mg(OH)_2$ and MgO also show very high activities for CO oxidation at ultralow temperatures.[17] This supports the statement that the presence of very small gold entities with sizes below 1 nm is not mandatory for highly active gold catalysts. However, so far, no other support than the magnesium-based system were found to be suitable for preparing such active gold catalyst. In addition to magnesium oxide and hydroxide, manganese oxides are among the most active catalyst supports for gold nanoparticles in CO oxidation, and it seemed worthwhile to investigate them more comprehensively for this reaction. Mn_2O_3 is generally considered to be the most favorable manganese oxide, while MnO_2 only shows moderate activity.[16,19]

In the following, we describe a series of manganese oxide-based gold catalysts prepared by the colloidal deposition method, which show unexpectedly high activity for the CO oxidation reaction at ultralow-temperatures below −80 °C. A specific reaction rate of 2.8 $mol_{CO} \cdot h^{-1} \cdot g_{Au}^{-1}$ was measured at a temperature as low as −85 °C, which is almost 30 times higher

than that of the most active Au/Mn$_2$O$_3$ catalyst (<0.098 mol$_{CO}$·h^{-1}·g$_{Au}$$^{-1}$).[16] Stability tests show the gold supported on MnO$_2$ nanowire catalyst to be stable for up to 70 h at 25 °C under normal conditions, which is even better than for the most active Co$_3$O$_4$ nanowire catalyst.[7] Detailed investigations reveal that the high surface area, the preparation method, as well as the presence of water molecules play important roles for the high activity. Furthermore, the Au/MnO$_2$ was also investigated in propene oxidation, and it proves to be very active and stable at rather low temperature (260 °C). These results show that the support effect is also very important in this reaction, which could provide new ideas for designing highly active catalysts.

2. EXPERIMENTAL SECTION

2.1. Catalyst Preparation. *2.1.1. Preparation of Manganese Oxide Support.* α-MnO$_2$ nanowires were prepared by modifying the established procedures.[20] For a typical synthesis, 2.25 g of MnSO$_4$·H$_2$O and 1.40 g of KMnO$_4$ were dissolved in 160 mL of distilled water at room temperature to form a homogeneous solution, which was then transferred into a 200 mL Teflon-lined stainless steel autoclave, sealed, and maintained at 160 °C for 12 h. The product was collected by filtration, washed with distilled water and ethanol, and finally dried in a 50 °C oven.

Highly ordered mesoporous β-MnO$_2$ was prepared by the nanocasting method with mesoporous silica SBA-15 as a hard template.[21,22] The Mn(NO$_3$)$_2$·4H$_2$O precursor was incorporated in the channels of mesoporous silica via an evaporation assisted impregnation process.[23,24] The mass ratio of precursor to silica pore volume was fixed to 2 g·cm^{-3}. The subsequent decomposition of the precursor was carried out in a muffle oven at 380 °C for 5 h with a ramp rate of 1 °C·min^{-1}. Finally, the mesoporous silica hard template was leached by hot NaOH solution (2 M, 100 mL, and 70 °C).

β-MnO$_2$ nanorod samples were prepared by a similar procedure to that used for the synthesis of α-MnO$_2$ nanowires. For a typical synthesis, 0.68 g of MnSO$_4$·H$_2$O and 1.31 g of (NH$_4$)$_2$S$_2$O$_8$ were dissolved in 160 mL of distilled water at room temperature to form a homogeneous solution, which was then transferred into a 200 mL Teflon-lined stainless steel autoclave, sealed, and maintained at 140 °C for 12 h. The subsequent steps were identical to those described for the synthesis of the α-MnO$_2$ nanowires.

Mn$_2$O$_3$ was prepared by thermal decomposition of MnCO$_3$ (Sigma-Aldrich) at 500 °C for 5 h under air with a ramp of 1 °C·min^{-1}.

2.1.2. Preparation of Au-Manganese Oxide Catalysts via the Colloidal Deposition Method.[10] In a typical preparation, the protecting agent PVA (poly vinyl alcohol, M_w = 1000, Aldrich, 80% hydrolyzed) was added to a 100 mg·L^{-1} aqueous HAuCl$_4$ solution (Au/PVA = 1.5/1 mg·mg^{-1}) at room temperature under vigorous stirring. The obtained solution was then left under stirring for 10 min. Subsequent rapid injection of an aqueous solution of NaBH$_4$ (0.1 mol·L^{-1}, Aldrich, 97%, Au/NaBH$_4$ = 1/5 mol·mol^{-1}) led to formation of a dark orange-brown solution, indicating the formation of gold sol. The manganese oxide supports were then added to the colloidal gold solution under stirring and kept in contact for 3–5 h. The gold content was adjusted to reach a loading of approximately 1 wt % if total adsorption occurred. All steps were carried out under exclusion of light, and Millipore water was used. The products were collected by centrifugation and washed thoroughly with Millipore water.

2.1.3. Preparation of Au-Manganese Oxide Catalysts via the Deposition Precipitation Method.[25] In a typical preparation (for about 1 wt % Au loading), 1.0 g of support powder was suspended in 100 mL of Millipore water. 0.205 mL of 0.25 mol/L HAuCl$_4$ aqueous solution and 0.308 g of urea were then added to the solution under stirring at room temperature. After that, the solution was heated to 90 °C and kept for 4 h under stirring. The products were collected by centrifugation and washed thoroughly with deionized water and dried in a 50 °C oven overnight before calcination at 300 °C for 4 h in air with a ramp rate of 1 °C·min^{-1}.

2.2. Characterization. The powder X-ray diffraction (XRD) patterns were recorded on a Stoe θ−θ diffractometer operating in reflection mode with Cu K$\alpha_{1,2}$ radiation and with a secondary graphite monochromator. The nitrogen adsorption−desorption measurements were performed on a NOVA 4200e instrument at 77 K. Prior to the measurements, all samples were degassed under vacuum for at least 6 h at 150 °C. The BET surface area was calculated from the data in a relative pressure range from 0.05−0.20. By using the Barrett−Joyner−Halenda (BJH) model, the pore volumes and pore size distributions were derived from the adsorption branches of the isotherms (normally desorption is recommended, but the desorption branches could be influenced by the tensile strength effect). High-resolution scanning electron microscope (HR-SEM) images and scanning transmission electron microscope (STEM) images were taken on a Hitachi S-5500 ultrahigh-resolution cold field emission scanning microscope with a Thermo Scientific NORAN System 7 X-ray Microanalysis unit at an acceleration voltage of 30 kV. STEM images were recorded on a Hitachi HD-2700 dedicated scanning transmission electron microscope operated at 200 kV equipped with an EDAX Octane T Ultra W EDX detector. Transmission electron microscopy (TEM) images were recorded with a Hitachi H-7100 at an acceleration voltage of 100 kV and high-resolution TEM with a Hitachi HF-2000 microscope equipped with a cold field emission gun and a Noran energy dispersive X-ray (EDX) unit at an acceleration voltage of 200 kV. X-ray photoelectron spectroscopy (XPS) measurements were performed with a Kratos His spectrometer with a hemispherical analyzer. The monochromatized Al X-ray source (E = 1486.6 eV) was operated at 15 kV and 15 mA. For narrow scans, an analyzer pass energy of 40 eV was applied. Hybrid mode was used as lens mode. The base pressure in the analysis chamber was 4 × 10^{-9} Torr. The binding energy scale was corrected for surface charging by use of the C 1s peak of contaminant carbon as reference at 285.0 eV. Temperature-programmed reduction (TPR) experiments were performed with an in-house constructed system, equipped with a thermal conductivity detector (TCD) to measure H$_2$ consumption. A 30 mg sample was reduced with a 4.5 vol % H$_2$/N$_2$ mixture (30 mL·min^{-1}) by heating up to 800 °C at a ramp rate of 10 °C·min^{-1}.

In situ Raman measurements were carried out with a 785 nm laser and a power of 15−29 mW with a Kaiser Optical Systems Inc. Raman spectrometer. The sample was placed in an *in situ* cell (Linkam 600) that could be heated to 500 °C and cooled to −100 °C. The sample was activated by heating to 300 °C with synthetic air (20 vol % O$_2$ and 80 vol % N$_2$ gas mixture) at a gas flow rate of 100 mL·min^{-1}. After dwelling for 30 min at that temperature, the sample was cooled to room temperature. Raman spectra were measured prior to activation, during heat treatment and after heat treatment.

Fourier transform infrared (FTIR) spectra were measured in a diffuse reflectance cell (Harrick system) equipped with CaF_2 windows on a Nicolet Magna 560 FTIR spectrometer using a mercury−cadmium−telluride (MCT)/A detector. After pretreatment of the catalysts (15 mg) in a gas flow of 1 vol % CO, 20 vol % O_2, and 79 vol % He (30 mL·min^{-1}) at 300 °C for 30 min, the reaction cell was cooled to −50, +20, or +100 °C in the N_2 stream. Then a background spectrum was collected via 256 scans at 4 cm^{-1} resolution. The catalyst was exposed to 1 vol % CO, 20 vol % O_2, and 79 vol % He (30 mL·min^{-1}), and diffuse reflectance Fourier transform (DRIFT) spectra were obtained by subtracting the background spectrum from subsequent spectra. DRIFT spectra during the pretreatment were also recorded by subtracting the background spectrum recorded at 25 °C under N_2 flow to monitor the activation process.

2.3. Catalytic Testing. The catalytic activity of catalysts for CO oxidation were measured in a plug flow reactor by use of defined amounts of catalyst (50 mg of catalyst, weight hour space velocity WHSV = 80 000 mL·h^{-1}·g$_{cat}$$^{-1}$) in a gas mixture of 1 vol % CO, 20 vol % O_2, and 79 vol % He (Air Liquid, 99.997% purity, H_2O content ~3 ppm) at a flow rate of 67 mL·min^{-1}. Catalysts were pressed, crushed, and sieved to the 250−500 μm size range and diluted with 200 mg of quartz sand; in the reactor the mixture was supported on a glass wool plug. The operation temperature was controlled with a thermocouple and could be adjusted in the range of −100 to +400 °C. Temperatures measured during the catalytic tests are always referred to the value measured with a second thermocouple placed in the catalyst bed. Before measurement, the catalysts were first pretreated *in situ* in the reaction gas at 300 °C for 30 min. For the experiments under dry conditions, the entire feed passed through a molecular sieve trap cooled to −78 °C (2-propanol/dry ice bath) before going into the reactor.

For a typical light-off run, in which the temperature was ramped, the reactor with catalyst was cooled to −100 °C prior to each experiment under a flow of He gas, which was then replaced by the reaction gas, after the base temperature had been reached. Then, the temperature was ramped with a rate of 2 °C·min^{-1} to the final temperature. The concentrations of CO_2 and CO were analyzed at the outlet of the reactor with nondispersive IR spectroscopy on two URAS 3E analyzers (Hartmann and Braun). Kinetic measurements were performed under differential conditions, with typically 5 mg of catalyst. Operation conditions: 100 mL·min^{-1}; WHSV = 1 200 000 mL·h^{-1}·g$_{cat}$$^{-1}$, 1 vol % CO, 20 vol % O_2 and He balance. The catalysts were pretreated in the reaction gas at 300 °C for 30 min and then cooled to the desired temperature with CO conversion below 15% and stabilized for 1 h. For measurement under dry conditions, the feed gas was passed through a molecular sieve trap cooled to −78 °C (2-propanol/dry ice bath) before going into the reactor.

For a typical steady-state experiment, 200 mg of catalyst was pretreated in the reaction gas at 300 °C for 30 min, then the system was cooled to +25 or −77 °C under He flow. The gas flow was then switched to the reaction gas with a flow rate of 50 mL·min^{-1} (WHSV = 15 000 mL·h^{-1}·g$_{cat}$$^{-1}$). The activity was recorded during the whole catalytic experiment.

The titration experiments were carried out in the same reactor in which the CO oxidation activities were tested, using 50 mg of catalyst. The catalysts were pretreated in the reaction gas (1 vol % CO, 20 vol % O_2, and 79 vol % He) at 300 °C for 10 min. Then the gas was switched to He to remove the O_2 gas

from the reactor. After the reactor was cooled to the desired temperature and kept there for 10 min, the catalysts were exposed to a stream of 1% CO in N_2 (from Air Liquide, 99.997% purity, H_2O content ~3 ppm) at a flow rate of 67 mL·min^{-1}. Online analysis was performed with nondispersive IR analyzers (URSA 3E), that allowed detection of CO and CO_2 in a nitrogen carrier gas without interference problems.

The propene oxidation activity of Au/α-MnO$_2$(NW) was measured in a plug flow reactor by use of defined amounts of catalyst (15 mg of catalyst, space velocity WHSV = 60 000 mL·h^{-1}·g$_{cat}$$^{-1}$) in a gas mixture of 1 vol % C_3H_6, 20 vol % O_2, and 79 vol % N_2 at a flow rate of 15 mL·min^{-1}. Catalysts were pressed, crushed, and sieved to the 250−500 μm size range. Before measurement, the catalysts were first activated *in situ* in the reaction gas at 300 °C for 30 min. The concentrations of C_3H_6 were analyzed at the outlet of the reactor by Fourier transform infrared (FTIR) spectroscopy, using a Thermo Electron Nicolet Avatar 370.

3. RESULTS AND DISCUSSION

The wide-angle XRD pattern of the hydrothermally synthesized α-MnO$_2$ nanowires (Figure 1a) confirms the phase purity of
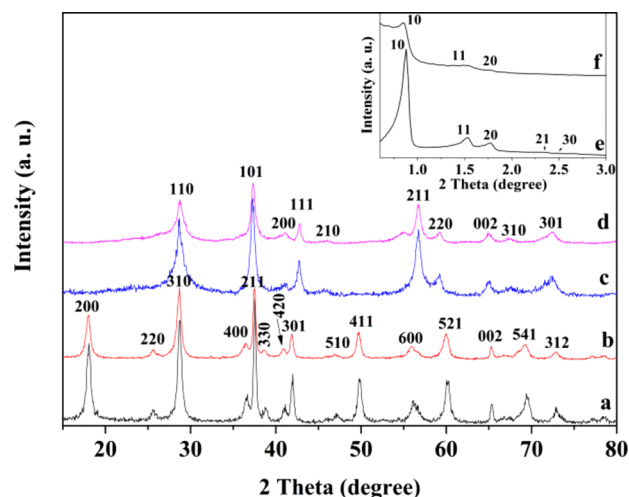

Figure 1. Wide-angle and low-angle (inset) XRD patterns of (a) α-MnO$_2$(NW) prepared by hydrothermal method, (b) Au/α-MnO$_2$(NW), (c) β-MnO$_2$(meso) nanocast from SBA-15, (d) Au/β-MnO$_2$(meso), (e) SBA-15 template, and (f) mesoporous β-MnO$_2$.

MnO$_2$ (α-MnO$_2$, PDF2 entry 44-0141). In contrast, use of the nanocasting method leads to the formation of the β-MnO$_2$ phase (PDF2 entry 24-0735) (Figure 1c). The low-angle XRD pattern (Figure 1f) of the mesoporous β-MnO$_2$ replica shows three well-resolved reflections, which can be indexed as (10), (11), and (20) reflections, consistent with the *p6m* symmetry characteristic for the two-dimensional hexagonal structure. The low angle diffraction peaks of β-MnO$_2$ are similar to that of SBA-15 (Figure 1e), indicating good replication of the template. The gold supported on MnO$_2$ is difficult to detect by XRD due to the low loading (Figure 1b,d).

TEM and bright field HR-STEM images (Figure S1a, c) of hydrothermally synthesized α-MnO$_2$ show a uniform nanowire morphology with diameters between 12−25 nm and lengths on the micrometer scale. All nanowires are grown with their main axis along the (100) direction. After loading with GNPs, the HR-SEM and dark field STEM images (Figure 2a,b) of the Au/

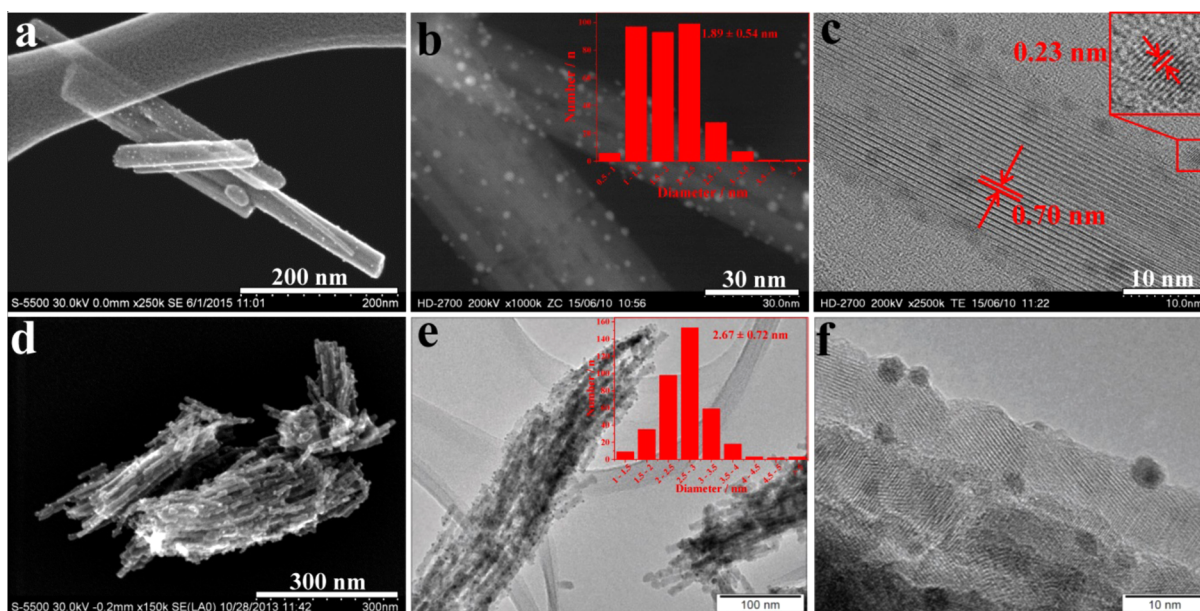**Figure 2.** (a) Dark field HR-SEM, (b) dark field HR-STEM, and (c) bright field HR-STEM images of Au/α-MnO$_2$(NW) prepared by the hydrothermal method; (d) HR-SEM and (e, f) HR-TEM images of Au/β-MnO$_2$(meso) prepared by the nanocasting method; the insets in (b) and (e) are size distributions of supported gold nanoparticles.
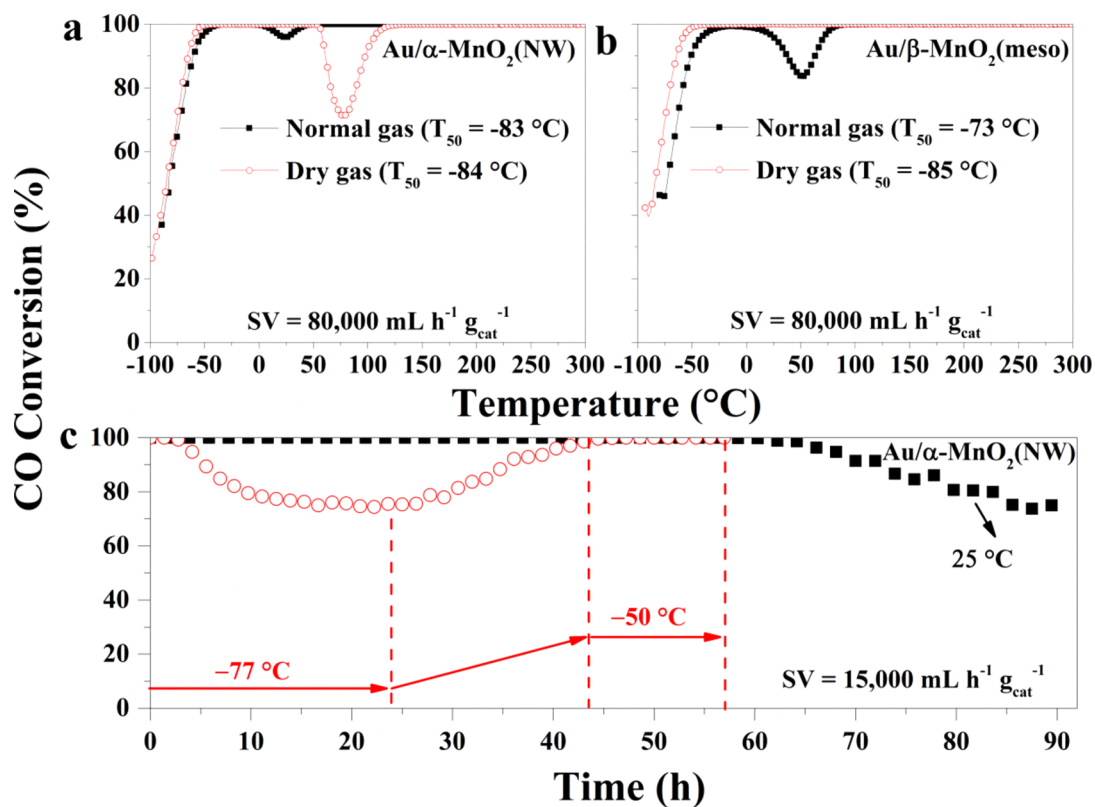

Figure 3. Temperature dependence of the activity for CO oxidation for (a) Au/α-MnO$_2$(NW) and (b) Au/β-MnO$_2$(meso). Operation conditions: 50 mg catalyst, 67 mL·min^{-1}; WHSV = 80 000 mL·h^{-1}·g$_{cat}$$^{-1}$, 1 vol % CO, 20 vol % O$_2$ and 79 vol % He. The catalysts were pretreated in the reaction gas at 300 °C for 30 min. (c) the catalytic stability of Au/α-MnO$_2$(NW) at +25 and −77 °C. Operation conditions: 200 mg catalyst, 50 mL·min^{-1}; WHSV = 15 000 mL·h^{-1}·g$_{cat}$$^{-1}$. The catalysts were pretreated in the reaction gas at 300 °C for 30 min. For measurement under dry conditions, the feed gas was passed through a molecular sieve trap cooled to −78 °C (2-propanol/dry ice bath) before going into the reactor.

α-MnO$_2$(NW) show highly dispersed small GNPs supported on the surface of α-MnO$_2$ nanowires. The particle size of GNPs ranges from 1 to 3 nm with an average size of about 1.9 nm. These values are quite similar to our previous reports[17] and

further prove the reproducibility of the colloidal deposition method. The bright field HR-STEM (Figure 2c) image clearly reveals the crystalline nature of both the nanowires and the GNPs. The contact between the GNPs and the α-MnO$_2$

nanowires appears to be very good, even immediately after deposition without a thermal treatment step. For mesoporous β-MnO$_2$, the TEM image (Figure S1b) shows a rod-like morphology, which is replicated from the SBA-15 template. After gold loading, the HR-SEM and TEM images (Figure 2d,e) of the Au/β-MnO$_2$(meso) show highly dispersed and small crystallites of gold with an average size of ca. 2.7 nm. This value is very close to that of Au/α-MnO$_2$(NW), indicating that the colloidal deposition method can eliminate the effect of the support to some extent. The HR-TEM image (Figure 2f) of Au/β-MnO$_2$(meso) clearly shows randomly oriented lattice fringes of the MnO$_2$ support, suggesting that the nanocast MnO$_2$ material has a highly crystalline structure. Most of the gold nanoparticles seem to be embedded in the pores of the MnO$_2$, indicating a good contact between the GNPs and the support. Nitrogen sorption data (not shown) evaluated by the Brunauer−Emmett−Teller (BET) method reveal specific surface areas of α-MnO$_2$ nanowires and mesoporous β-MnO$_2$ of 45 and 61 m^2·g^{-1}, respectively (Table S1). These values are relatively high, if the high density of the oxides and the low amount of micropores are taken into account. After gold loading, the surface areas decrease to 40 and 50 m^2·g^{-1}, which is still much higher than the specific surface areas of commercial manganese oxides (Table S1).

The catalytic activities of the catalysts for CO oxidation were measured in a plug flow reactor using a gas mixture of 1 vol % CO, 20 vol % O$_2$, and 79 vol % He. The results are shown in Figure 3 and summarized in Table S1. Surprisingly, both Au/α-MnO$_2$(NW) and Au/β-MnO$_2$(meso) show extremely high activities at low temperatures. The Au/α-MnO$_2$(NW) catalyst under normal conditions (with about 3 ppm of H$_2$O) at a space velocity of 80 000 mL·h^{-1}·g$_{cat}^{-1}$ shows a CO conversion of around 37% at -90 °C (Figure 3a). With increasing temperature the CO conversion increases rapidly to 90% below -60 °C, and slowly reaches 100% CO conversion at around -34 °C. 50% CO conversion (T_{50}) is achieved at a temperature of -83 °C. Interestingly, the CO conversion slightly drops at about -8 °C and reaches a minimum at 24 °C with a CO conversion of 96%. Then the CO conversion again increases to 100% at around 48 °C. This "U-shaped" curve has been observed for several times in other systems,[8,17,26] indicating negative apparent activation energies, which had been attributed to the influence of water. However, this phenomenon had not been reported for Au/MnO$_2$ catalysts. Under dry conditions (H$_2$O below 1 ppm), the Au/α-MnO$_2$(NW) catalyst shows a similar activity at low temperatures with T_{50} around -84 °C. However, the minimum of the "U-shaped" curve shifts slightly to higher temperatures with a turning point at 77 °C and 71% CO conversion. These results further confirm the conclusion that moisture could enhance the catalytic activity of gold catalysts at around room temperature.[27,28] The temperature dependence of CO conversion using Au/β-MnO$_2$(meso) catalyst is given in Figure 3b. Under normal conditions, a "U-shaped" curve similar to that of Au/α-MnO$_2$(NW) catalyst is observed. A T_{50} of -73 °C and a turning point around 84 °C with a CO conversion of 84% are achieved. However, under dry conditions, this "U-shaped" curve is not observed and a T_{50} of -85 °C is observed. This may be due to the higher activity of this catalyst under dry conditions.

Light-off curves measured under transient conditions may give misleading results if steady states are reached slowly. Therefore, activity tests under stationary conditions for a Au/α-

MnO$_2$(NW) catalyst were performed at different temperatures. Figure 3c shows the catalytic stability of Au/α-MnO$_2$(NW) at 25 °C (black square) with a space velocity of 15 000 mL·h^{-1}·g$_{cat}^{-1}$ under normal conditions. This experiment reveals very high stability: Deactivation does not start before $\sim$70 h, and even after 90 h the CO conversion is still higher than 80%. This stability is significantly better than that of the most active Co$_3$O$_4$ nanorod catalyst.[7] At-77 °C, no obvious deactivation was visible during the first 3 h of operation. After this, the CO conversion decreased slowly to 75% within 24 h. After that, the temperature increased from -77 to -50 °C within another 20 h with the sublimation of the dry ice in the thermostatic bath and the CO conversion increases back to 100% and remains stable for more than 20 h. No further deactivation was observed within 58 h. Even under steady-state conditions at -77 °C, the specific rate still exceeds 0.45 mol$_{CO}$·h^{-1}·g$_{Au}^{-1}$, almost four times higher than that observed for the most active Au/Mn$_2$O$_3$ catalyst reported in the literature.[16] Overall, the results of the steady-state analysis confirmed the high activity of Au/α-MnO$_2$(NW) catalyst for low-temperature CO oxidation.

The apparent activation energies of CO oxidation over various Au/MnO$_2$ catalysts both under normal and dry gas conditions are shown in Figure 4 (determined at differential
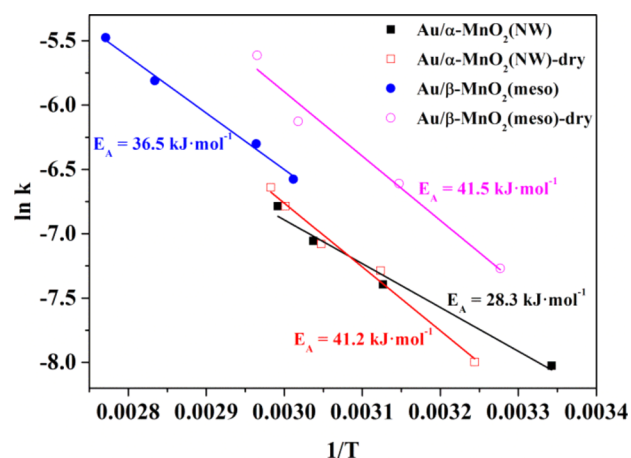

Figure 4. Arrhenius plots and crosspsonding activation energy (E_A) of Au/α-MnO$_2$(NW) and Au/β-MnO$_2$(meso). Operation conditions: 5 mg catalyst, 100 mL·min^{-1}; WHSV = 1 200 000 mL·h^{-1}·g$_{cat}^{-1}$, 1 vol % CO, 20 vol % O$_2$ and He balance. The catalysts were pretreated in the reaction gas at 300 °C for 30 min and then cooled down to desired temperature with CO conversion below 15% and stabilized for 1 h. For measurement under dry conditions, the feed gas was passed through a molecular sieve trap cooled to -78 °C (2-propanol/dry ice bath) before going into the reactor.

CO conversion below 15%, therefore the slightly different temperature ranges for the different catalysts). Au/α-MnO$_2$(NW) under normal conditions shows an apparent activation energy of 28 kJ·mol^{-1}. Under dry conditions, the apparent activation energy is 41 kJ·mol^{-1}, suggesting a positive influence of water. Au/β-MnO$_2$(meso) shows an almost identical apparent activation energy of 42 kJ·mol^{-1} as that of Au/α-MnO$_2$(NW) measured under dry conditions. Considering the lower gold loading amount, the Au/β-MnO$_2$(meso) catalyst has a somewhat higher catalytic activity, corresponding very well with the light-off results. Under normal condition, Au/β-MnO$_2$(meso) shows an apparent activation energy of 37 kJ·mol^{-1}.

Generally, MnO_2 is neither considered a good catalyst in itself nor a good support for low-temperature CO oxidation catalysts.[19,29] The best Au-manganese oxide catalyst for low-temperature CO oxidation reported so far is Au/Mn_2O_3 (Au loading 4.9 wt %), which shows a T_{50} of ∼− 63 °C at a space velocity of 60 000 $mL \cdot h^{-1} \cdot g_{cat}^{-1}$.[16] In order to understand the origin of the unexpectedly high activity of the Au-MnO_2 system, the materials were characterized systematically. The surface compositions and the chemical states of the catalysts were analyzed by XPS (Figure 5).
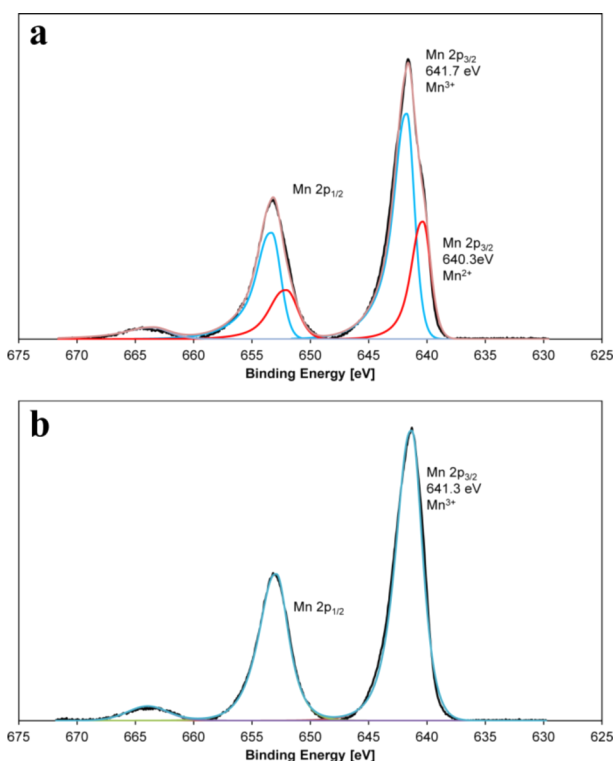

Figure 5. Mn 2p XPS-spectra of (a) Au/α-MnO_2(NW) and (b) Au/β-MnO_2(meso).

The evaluation of the Mn 2p narrow scans allows the assignment of the oxidation state of Mn.[30−32] Generally, Mn 3s also should be considered,[33] however, in our cases, the Au 4f signal overlaps with the Mn 3s. Au/α-MnO_2(NW) shows a broad peak at 638−648 eV, which can be assigned to a mixed oxidation state of Mn^{2+} and Mn^{3+}, indicating that the surface manganese species are partially reduced during the catalyst preparation process by the excess of $NaBH_4$. Also the presence of Mn^{4+} cannot be excluded. For Au/β-MnO_2(meso), only Mn^{3+} was detected on the catalyst surface. Au 4f XPS results reveal that the Au oxidation state for both catalysts is Au^0. The XPS results suggest that the surface manganese species were at least partially reduced, which may lead to formation of Mn^{4+}/ $Mn^{3+/2+}$ redox couples on the catalysts surface and therefore promote the catalytic activity of these catalysts for CO oxidation.

It is known that the adsorption and activation of molecular oxygen are important steps which govern the activity of gold catalysts for CO oxidation. The formation of adsorbed reactive oxygen species, such as superoxide ions (O^{2-}), might be correlated to the presence of surface oxygen vacancies on the metal oxide support or at the metal−support interface.

Therefore, CO titration experiments in the absence of oxygen (1 vol % CO in N_2) were performed. This allows us to assess the extent of the supply of oxygen stored on the catalysts. Figure 6 shows the transient response of the CO_2 and CO evolution over pretreated
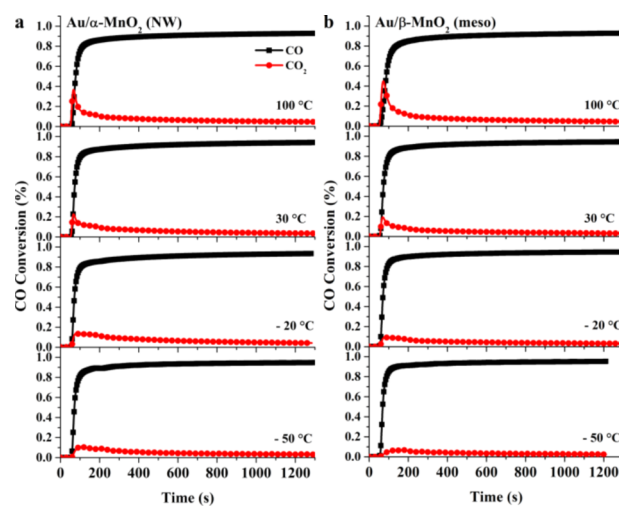

Figure 6. CO_2 response in the CO titration experiments of the pretreated (1 vol % CO, 20 vol % O_2, and 79 vol % He) Au/α-MnO_2(NW) (a) and Au/β-MnO_2(meso) (b) catalysts at temperatures of −50, −20, +30, and +100 °C. All the above experiments were carried out under normal conditions. Catalyst, 50 mg; reaction gas, 1 vol % CO in N_2; flow rate, 67 $mL \cdot min^{-1}$.

Au/α-MnO_2(NW) and Au/β-MnO_2(meso) catalysts at different temperatures. For Au/α-MnO_2(NW), the ability to provide reactive oxygen is rather high at low-temperature (−50 °C). High CO_2 evolution with a maximum (CO_2 concentration 0.11%) at 101 s after exposure to CO is observed. The initial CO_2 response is indicative for a fast reaction, proceeding via rapid adsorption of CO, followed by the reaction of CO with the reactive oxygen on the catalyst surface. It is noticed that, even after 1200 s, substantial amounts of CO_2 were still produced. At−20 °C, a CO_2 response maximum was observed after 79 s with an even higher CO_2 concentration (0.14%) than that observed at −50 °C. The CO_2 evolution decreased gradually to the same level observed at −50 °C after 1200 s. At 30 and 100 °C, the CO_2 concentration peaked both after 67 s with CO_2 concentrations of 0.23% and 0.37%, respectively. CO titration results of Au/β-MnO_2(meso) show a similar trend and CO_2 evolution level. However, the oxygen consumption normalized to surface area (Table S2) shows much higher values for Au/α-MnO_2(NW) than for Au/β-MnO_2(meso) at −50, −20, and +30 °C, suggesting the Au/α-MnO_2(NW) contains more reactive oxygen per unit surface area at low temperatures. This corresponds well to the activation energy results calculated from the Arrhenius plots.

In situ Raman spectroscopy was used to detect possible reactive oxygen species on the catalyst surface, the results are shown in Figure S2. At room temperature, prior to heat treatment, only bands at 635, 577, and 467 cm^{-1} were observed for Au/α-MnO_2(NW), which are assigned to the stretching mode at metal−oxygen chains in α-MnO_2.[34] After heat treatment, the bands at 635 and 577 cm^{-1} were shifted to 641 and 581 cm^{-1}, respectively, but no additional Raman bands could be observed. Hence, no features of peroxide or

superoxide, which are expected at about 1123 and 883 cm^{-1},[35,36] were observed both before and after heat treatment under air atmosphere for this sample. In contrast, for Au/β-MnO$_2$(meso), next to the Raman bands at 651, 573, and 467 cm^{-1}, due to metal−oxygen stretching vibrations, weak bands at 1171 and 754 cm^{-1} were observed, of which the former may be assigned to superoxide species. However, the intensity of the possible superoxide species is too poor to be reliably distinguished from the noise. Therefore, peroxide and/or superoxide species are most likely not the origin of the unexpectedly high activity.

Bongiorno et al.[37] found that water molecules can enhance the catalytic activity of supported gold catalysts for CO oxidation. *In situ* DRIFT spectroscopy (Figure S3) was used to detect possible water, CO, and CO$_2$ species adsorbed on the surfaces of Au/α-MnO$_2$(NW) catalysts at different temperatures. However, the spectra under simulated reaction conditions at different temperatures only reveal the characteristic gas-phase bands of CO at 2111 and 2173 cm^{-1} and CO$_2$ at 2335 and 2363 cm^{-1}, no adsorbed CO and CO$_2$ were detected. Thus, no additional information on surface species could be inferred from the *in situ* DRIFT results.

Results obtained by H$_2$-TPR experiments are presented in Figure 7. Three typical peaks can be observed for all Au-MnO$_2$
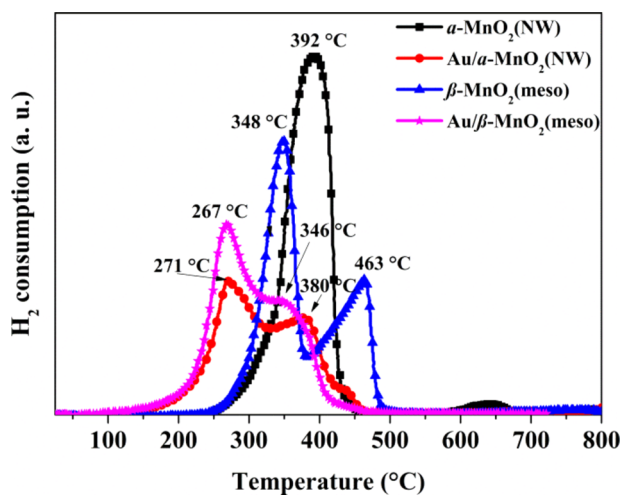

Figure 7. H$_2$-TPR profile of α-MnO$_2$(NW), Au/α-MnO$_2$(NW), β-MnO$_2$(meso), and Au/β-MnO$_2$(meso). Operation conditions: 30 mg sample; gas flow: 30 mL·min^{-1} (4.5 vol % H$_2$ in N$_2$); ramp rate: 10 °C·min^{-1}.

catalysts. The sharp signal around 271 °C observed for Au/α-MnO$_2$(NW) can be attributed to the reduction of MnO$_2$ to Mn$_3$O$_4$. It is much lower than that at 392 °C of pure α-MnO$_2$ nanowires, indicating that the GNPs promote the reduction of MnO$_2$. The second broad peak around 380 °C is attributed to the consecutive reduction of Mn$_3$O$_4$ to MnO. Moreover, a third broad shoulder can be observed at above 400 °C, which can be attributed to a further reduction of MnO to other manganese oxide species. The reduction peaks observed for Au/β-MnO$_2$(meso) are also appearing at much lower temperatures than those of pure mesoporous β-MnO$_2$.

It has been demonstrated that the support has a substantial effect on the activity of the catalysts in CO oxidation.[27,38] The oxygen availability from the support, the interactions between the support and GNPs, the oxygen species, and many other factors are essential for the catalytic activities. In order to understand the influence of support and catalyst preparation methods in more detail, a series of gold catalysts with various manganese oxides as support was prepared by colloidal deposition (CD) or by deposition precipitation (DP) methods (Table S1). β-MnO$_2$ nanorods with a surface area of 14 m^2·g^{-1} were prepared by the hydrothermal method (Figure S4). The Au/β-MnO$_2$(NR) catalyst shows a gold particle size of 1.95 nm, similar to that of the Au/β-MnO$_2$(meso) catalyst (Figure S5). The CO oxidation results shows a T_{50} of −36 °C, which is substantially higher than that of Au/β-MnO$_2$(meso), indicating that the surface area of the support could influence the catalytic activity. Commercial manganese oxides (MnO$_2$, Mn$_2$O$_3$, and Mn$_3$O$_4$) with low surface areas were also used as supports of GNPs. They all show poor catalytic activity compared to the high surface area materials used in this work (Figure S6−9, Table S1). DP is another very important method to prepare GNPs with small size. Cao and co-workers[16] used the DP method to prepare Au/Mn$_2$O$_3$ catalyst, which show high activity for CO oxidation at low temperatures. To understand the influence of the GNPs loading method, we prepared Au/α-MnO$_2$(NW)-DP catalysts by the DP method. No GNPs are observed in the TEM images (Figure S10), and XRD shows the presence of large Au particles. This indicates that the DP method is not suitable for a successful loading of GNPs on high surface area MnO$_2$ catalyst. The CO oxidation results of this Au/α-MnO$_2$(NW)-DP catalyst shows a T_{50} of 175 °C under normal conditions, which is much higher than that of Au/α-MnO$_2$(NW). However, the CO oxidation activity of the Au/Mn$_2$O$_3$-DP catalyst prepared by the DP method is much higher (T_{50} of −25 °C, Figure S11, 12). Considering the relatively low gold content, this activity is comparable with the literature value,[19] suggesting that the CO oxidation results measured on different devices in different groups are comparable. An Au/Mn$_2$O$_3$ catalyst was also prepared by the CD method. TEM images show a gold particle size of 2.37 nm (Figure S13) and further prove the reproducibility of the GNP synthesis by the CD method. However, the T_{50} is as high as 64 °C (Figure S14 and Table S1), substantially higher than that of Au/α-MnO$_2$(NW) and Au/Mn$_2$O$_3$-DP, but still better than that of most of the catalysts supported on commercial oxides. These results suggest that not only the surface area of the support might influence the catalytic activity of gold catalyst, but also the catalyst preparation method. Higher surface areas normally result in better catalytic activity; by using the CD method, highly active catalysts can be prepared with both α- and β-MnO$_2$ as supports, whereas the DP method is only suitable for the preparation of active Mn$_2$O$_3$, probably because in the DP method, no surface reduction of the MnO$_2$ takes place due to the absence of NaBH$_4$ (Figure S15).

The system Au/α-MnO$_2$(NW) was also examined for the oxidation of propene, one of the components in automotive exhaust gas (Figure 8). The conversion of propene reached ~100% at 280 °C at a space velocity of 60 000 mL·h^{-1}·g$_{cat}^{-1}$. Considering the higher space velocity and lower Au loading amount, this result is at least comparable with the most active gold catalyst usually used for this reaction (catalyst: 4.5 wt % Au/CeO$_x$/Al$_2$O$_3$; reaction gas: C$_3$H$_6$/O$_2$/He = 0.4/3.6/96; WHSV = 9 000 mL·h^{-1}·g$_{cat}^{-1}$; the 95% C$_3$H$_6$ conversion temperature is 224 °C).[39] Furthermore, this catalyst also shows a very high stability at constant conditions; no obvious deactivation was observed within 15 h at 260 °C with a propene conversion around 96%.

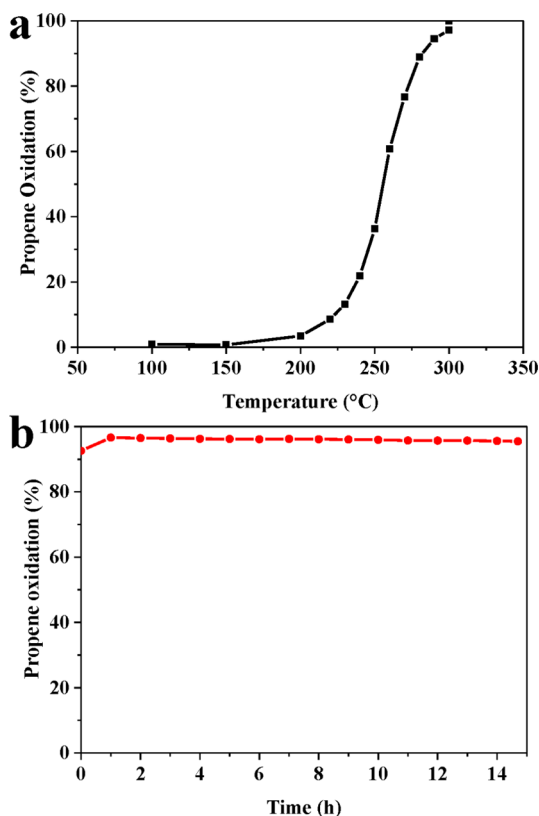**Figure 8.** (a) Temperature dependence and (b) the catalytic stability at 260 °C of Au/α-MnO$_2$(NW) catalyst for propene oxidation. Operation conditions: 15 mg catalyst, 15 mL·min^{-1}; WHSV = 60 000 mL·h^{-1}·g$_{cat}$$^{-1}$, 1 vol % C$_3H_6$, 20 vol % O$_2$ and N$_2$ balance. The catalysts were pretreated in the reaction gas at 300 °C for 30 min.

4. CONCLUSION

A series of different gold/manganese oxide catalysts were studied for their activity in CO oxidation. Particularly, we have synthesized gold catalysts by the colloidal deposition method on both hydrothermally derived α-MnO$_2$ nanowires and nanocast highly ordered mesoporous β-MnO$_2$ nanowire arrays. Both materials have uniform particle crystallinity, high surface areas and similar gold particle sizes. These gold catalysts show unexpectedly high activity in CO oxidation at ultralow-temperature (below −80 °C) and very good stability at 25 °C (>70 h) under normal conditions, as well as in low temperature propene oxidation (260 °C). A series of control experiments with various manganese oxides and different gold loading methods allowed the investigation of the influence of support effects and the preparation method. The results reveal that the high surface area of the manganese dioxide supports is beneficial for preparing high performance catalyst. The colloidal deposition method is the method of choice for the synthesis of highly active gold catalysts with MnO$_2$ as support, whereas deposition precipitation is more suitable for Mn$_2$O$_3$. Furthermore, on the basis of extensive catalyst characterization under both *in situ* and *ex situ* (after use) conditions, we identified the reduction of surface Mn^{4+} during catalyst preparation, and adsorption of H$_2$O molecules on the surface of the catalyst as the origin of the high catalytic activity. However, also other factors, such as differences in defect concentration and types of defects for different supports and synthesis pathways may also contribute to activity differences.

■ ASSOCIATED CONTENT

Ⓢ Supporting Information

The Supporting Information is available free of charge on the ACS Publications website at DOI: 10.1021/jacs.6b04251.

Additional results of XRD, TEM, STEM, Raman, DRIFT, and CO oxidation (PDF)

■ AUTHOR INFORMATION

Corresponding Author
*E-mail: schueth@mpi-muelheim.mpg.de. Fax: +49 208 3062995. Tel: +49 208 3062373

Notes
The authors declare no competing financial interest.

■ REFERENCES

(1) Haruta, M.; Yamada, N.; Kobayashi, T.; Iijima, S. *J. Catal.* **1989**, *115*, 301.
(2) Hashmi, A. S. K.; Hutchings, G. J. *Angew. Chem., Int. Ed.* **2006**, *45*, 7896.
(3) Haruta, M. *CATTECH* **2002**, *6*, 102.
(4) Corma, A.; Garcia, H. *Chem. Soc. Rev.* **2008**, *37*, 2096.
(5) Liu, X.; He, L.; Liu, Y.-M.; Cao, Y. *Acc. Chem. Res.* **2014**, *47*, 793.
(6) Yan, W. F.; Mahurin, S. M.; Pan, Z. W.; Overbury, S. H.; Dai, S. *J. Am. Chem. Soc.* **2005**, *127*, 10480.
(7) Xie, X. W.; Li, Y.; Liu, Z. Q.; Haruta, M.; Shen, W. J. *Nature* **2009**, *458*, 746.
(8) Jia, C.-J.; Schwickardi, M.; Weidenthaler, C.; Schmidt, W.; Korhonen, S.; Weckhuysen, B. M.; Schüth, F. *J. Am. Chem. Soc.* **2011**, *133*, 11279.
(9) An, K.; Alayoglu, S.; Musselwhite, N.; Plamthottam, S.; Melaet, G.; Lindeman, A. E.; Somorjai, G. A. *J. Am. Chem. Soc.* **2013**, *135*, 16689.
(10) Comotti, M.; Li, W. C.; Spliethoff, B.; Schüth, F. *J. Am. Chem. Soc.* **2006**, *128*, 917.
(11) Herzing, A. A.; Kiely, C. J.; Carley, A. F.; Landon, P.; Hutchings, G. J. *Science* **2008**, *321*, 1331.
(12) Liu, Y.; Jia, C.-J.; Yamasaki, J.; Terasaki, O.; Schüth, F. *Angew. Chem., Int. Ed.* **2010**, *49*, 5771.
(13) Carrettin, S.; Concepcion, P.; Corma, A.; Nieto, J. M. L.; Puntes, V. F. *Angew. Chem., Int. Ed.* **2004**, *43*, 2538.
(14) Guzman, J.; Carrettin, S.; Corma, A. *J. Am. Chem. Soc.* **2005**, *127*, 3286.
(15) Haruta, M.; Tsubota, S.; Kobayashi, T.; Kageyama, H.; Genet, M. J.; Delmon, B. *J. Catal.* **1993**, *144*, 175.
(16) Wang, L.-C.; Huang, X.-S.; Liu, Q.; Liu, Y.-M.; Cao, Y.; He, H.-Y.; Fan, K.-N.; Zhuang, J.-H. *J. Catal.* **2008**, *259*, 66.
(17) Jia, C.-J.; Liu, Y.; Bongard, H.; Schüth, F. *J. Am. Chem. Soc.* **2010**, *132*, 1520.
(18) Cunningham, D. A. H.; Vogel, W.; Kageyama, H.; Tsubota, S.; Haruta, M. *J. Catal.* **1998**, *177*, 1.
(19) Wang, L.-C.; Liu, Q.; Huang, X.-S.; Liu, Y.-M.; Cao, Y.; Fan, K.-N. *Appl. Catal., B* **2009**, *88*, 204.
(20) Wang, X.; Li, Y. D. *Chem. - Eur. J.* **2003**, *9*, 300.
(21) Zhao, D. Y.; Feng, J. L.; Huo, Q. S.; Melosh, N.; Fredrickson, G. H.; Chmelka, B. F.; Stucky, G. D. *Science* **1998**, *279*, 548.
(22) Zhao, D. Y.; Huo, Q. S.; Feng, J. L.; Chmelka, B. F.; Stucky, G. D. *J. Am. Chem. Soc.* **1998**, *120*, 6024.
(23) Tian, B. Z.; Liu, X. Y.; Yang, H. F.; Xie, S. H.; Yu, C. Z.; Tu, B.; Zhao, D. Y. *Adv. Mater.* **2003**, *15*, 1370.
(24) Gu, D.; Schüth, F. *Chem. Soc. Rev.* **2014**, *43*, 313.
(25) Zanella, R.; Giorgio, S.; Henry, C. R.; Louis, C. *J. Phys. Chem. B* **2002**, *106*, 7634.

(26) Gu, D.; Jia, C.-J.; Weidenthaler, C.; Bongard, H.-J.; Spliethoff, B.; Schmidt, W.; Schüth, F. *J. Am. Chem. Soc.* **2015**, *137*, 11407.

(27) Kung, M. C.; Davis, R. J.; Kung, H. H. *J. Phys. Chem. C* **2007**, *111*, 11767.

(28) Haruta, M. *Faraday Discuss.* **2011**, *152*, 11.

(29) Liang, S.; Bulgan, F. T. G.; Zong, R.; Zhu, Y. *J. Phys. Chem. C* **2008**, *112*, 5307.

(30) Nesbiti, H. W.; Banerjee, D. *Am. Mineral.* **1998**, *83*, 305.

(31) Ardizzone, S.; Bianchi, C. L.; Tirelli, D. *Colloids Surf., A* **1998**, *134*, 305.

(32) Moses Ezhil Raj, A.; Grace Victoria, S.; Bena Jothy, V.; Ravidhas, C.; Wollschläger, J.; Suendorf, M.; Neumann, M.; Jayachandran, M.; Sanjeeviraja, C. *Appl. Surf. Sci.* **2010**, *256*, 2920.

(33) Galakhov, V. R.; Demeter, M.; Bartkowski, S.; Neumann, M.; Ovechkina, N. A.; Kurmaev, E. Z.; Lobachevskaya, N. I.; Mukovskii, Y. M.; Mitchell, J.; Ederer, D. L. *Phys. Rev. B: Condens. Matter Mater. Phys.* **2002**, *65*, 113102.

(34) Gao, T.; Fjellvag, H.; Norby, P. *Anal. Chim. Acta* **2009**, *648*, 235.

(35) Pushkarev, V. V.; Kovalchuk, V. I.; d'Itri, J. L. *J. Phys. Chem. B* **2004**, *108*, 5341.

(36) Carrettin, S.; Hao, Y.; Aguilar-Guerrero, V.; Gates, B. C.; Trasobares, S.; Calvino, J. J.; Corma, A. *Chem. - Eur. J.* **2007**, *13*, 7771.

(37) Bongiorno, A.; Landman, U. *Phys. Rev. Lett.* **2005**, *95*, 106102.

(38) Schüth, F. *Phys. Status Solidi B* **2013**, *250*, 1142.

(39) Gluhoi, A. C.; Bogdanchikova, N.; Nieuwenhuys, B. E. *J. Catal.* **2005**, *229*, 154.